https://dx.doi.org/10.4314/dujopas.v12i1e.12
ISSN (Print): 2476-8316
ISSN (Online): 2635-3490
Dutse Journal of Pure and Applied Sciences (DUJOPAS), *Vol.12 No. 1e March 2026*

Comparative Pyrolysis Kinetics of Oil Palm Biomass Residues Via Thermogravimetric Analysis (TGA)

A.A Safana*, Mustapha Shehu, Lawan Haruna, Ahmad Muhammed Nazir and Muzzambilu Sa'adu

Federal University, Dutse,
Department of Physics,
Dutse, Jigawa, State,
Nigeria.

Email: aa.safana@fud.edu.ng

Abstract
This study investigates the pyrolysis kinetics of three oil palm biomass residues, empty fruit bunch (EFB), mesocarp fiber (MF), and palm kernel shell (PKS), using thermogravimetric analysis (TGA). Model-free methods including Kissinger-Akahira-Sunose (KAS) and Flynn-Wall-Ozawa (FWO), along with the model-fitting Coats-Redfern (CR) approach, were employed to determine kinetic parameters. The maximum activation energies obtained were 213.38 kJmol^{-1}, 210.78 kJmol^{-1}, and 193.35 kJmol^{-1}, for EFB, MF and PKS respectively, using the KAS method at conversion factors of 0.7, 0.4, and 0.7, respectively. PKS demonstrated the lowest activation energy, indicating more favorable decomposition characteristics. The CR method revealed that first-order (F1) kinetics dominated the reaction mechanism for EFB and MF, while second-order (F2) kinetics prevailed for PKS, correlating with their respective cellulose and lignin contents. Among diffusion models, the three-way transport Jander equation (D3) exhibited the lowest activation energies (35.50–37.47 kJmol^{-1}), suggesting its significance in char combustion. These findings provide essential kinetic data for optimizing thermochemical conversion processes of oil palm biomass residues.

Keywords: TGA, pyrolysis kinetics, oil palm biomass.

INTRODUCTION

The increasing global demand for renewable energy sources has intensified research into biomass conversion technologies. Biomass, particularly agricultural residues, represents a sustainable and carbon-neutral alternative to fossil fuels (Nussbaumer, 2003; Saidur *et al.*, 2011) Among various biomass sources, oil palm industry residues constitute a significant feedstock due to their abundance in tropical regions. The oil palm industry generates substantial quantities of lignocellulosic waste including empty fruit bunches (EFB), mesocarp fiber (MF), and palm kernel shells (PKS), which possess considerable potential for thermochemical conversion into valuable energy products (Abdullah and Sulaiman, 2013; Sulaiman and Abdullah, 2011).

Pyrolysis, a thermochemical decomposition process occurring in the absence of oxygen, has emerged as a promising technology for converting biomass into bio-oil, biochar, and syngas (Bridgwater, 2012; Damartzis and Zabaniotou, 2011). Understanding the thermal decomposition behavior and kinetic mechanisms of biomass pyrolysis is crucial for process optimization, reactor design, and product yield prediction (Di Blasi, 2008; Cai *et al.*, 2013). The kinetic parameters, particularly activation energy and pre-exponential factors, serve as

**Author for Correspondence*

fundamental indicators of the energy requirements and reaction rates during thermal conversion (Vyazovkin *et al.,* 2011).

Thermogravimetric analysis (TGA) has become the standard technique for investigating biomass pyrolysis kinetics due to its precision in measuring mass changes as a function of temperature and time (White *et al*., 2011). TGA enables researchers to derive kinetic parameters through both model-fitting and model-free (isoconversional) methods. Model-free approaches have gained preference over model-fitting techniques due to their independence from assumed reaction mechanisms, thereby minimizing errors associated with inappropriate model selection (Vyazovkin *et al.,* 2011; Mishra and Bhaskar, 2014).

Several researchers have investigated the pyrolysis kinetics of various biomass feedstocks. Islam *et al.,* (2015) examined the thermal decomposition of Karanj fruit hulls, revealing that lower activation energies indicate faster volatile decomposition. Slopiecka *et al.* (2011) conducted kinetic studies on poplar wood using thermogravimetric analysis, while Li *et al.* (2017) investigated the co-combustion behavior of municipal solid waste and biomass briquettes under different atmospheres. For oil palm biomass specifically, Safana *et al.* (2019) investigated the pyrolysis kinetics of palm shell and EFB using TGA with KAS and FWO isoconversional methods, reporting maximum activation energies of 213.38 and 193.35 $kJmol^{-1}$ for EFB and palm shell, respectively, confirming that shell with lower activation energy is a more favorable biomass for biofuels applications. Luangkiattikhun *et al.* (2008) similarly studied non-isothermal TGA of oil-palm solid wastes and reported the distinct multi-stage thermal decomposition profiles of these residues. However, comprehensive comparative studies incorporating MF alongside EFB and PKS, and employing multiple kinetic methods simultaneously, remain limited.

The complexity of biomass pyrolysis arises from the heterogeneous nature of lignocellulosic materials, comprising cellulose, hemicellulose, and lignin, each decomposing at different temperature ranges (Yang *et al.,* 2004). The thermal degradation typically occurs in multiple stages, with each component contributing distinct characteristics to the overall decomposition profile. Furthermore, the kinetic behavior varies significantly among different biomass types depending on their composition, structure, and physical properties (Chen *et al.,* 2014).

The present study aims to conduct a comprehensive kinetic analysis of three major oil palm biomass residues (EFB, MF, and PKS) using multiple kinetic methods, extending the work of Safana *et al.* (2019) by including MF as a third biomass and applying the CR model-fitting approach alongside the isoconversional methods. Specifically, this research employs the Kissinger-Akahira-Sunose (KAS) (Kissinger, 1957; Akahira and Sunose, 1971) and Flynn-Wall-Ozawa (FWO) (Flynn and Wall, 1966; Ozawa, 1965) model-free methods, complemented by the Coats-Redfern (CR) (Coats and Redfern, 1964) model-fitting approach. The findings will contribute to the optimization of pyrolysis processes and the efficient utilization of oil palm industry waste for sustainable energy production (Abdullah and Sulaiman, 2013; Sulaiman and Abdullah, 2011).

METHODOLOGY

The thermal decomposition of biomass during pyrolysis follows classical chemical kinetics principles (White *et al.,* 2011; Vyazovkin *et al.,* 2011). The overall rate equation for the conversion process is expressed through the Arrhenius relationship:

$$\frac{d\alpha}{dt} = k(T)f(\alpha) \quad (1)$$

where α represents the degree of conversion, k(T) is the temperature-dependent rate constant, and f(α) is a function dependent on the reaction mechanism. The conversion degree is calculated from thermogravimetric data as (Safana *et al.,* 2019):

$$\alpha = \frac{(m_i - m_t)}{(m_i - m_f)} \quad (2)$$

where m_i is the initial sample mass (mg), m_f is the final mass (mg), and m_t is the mass at temperature T (mg).
The temperature-dependent rate constant follows the Arrhenius equation:

$$k(T) = Aexp^{\left(-\frac{E}{RT}\right)} \quad (3)$$

where A is the pre-exponential factor (min^{-1}), E is the activation energy ($kJmol^{-1}$), R is the universal gas constant (8.314 $Jmol^{-1}K^{-1}$), and T is the absolute temperature (K) (Cai *et al.,* 2013).
For uniform kinetics, the reaction model can be described as:

$$f(\alpha) = (1-\alpha)^n \quad (4)$$

where n is the reaction order. Combining equations (1), (3), and (4) yields:

$$\frac{d\alpha}{dt} = Aexp^{\left(-\frac{E}{RT}\right)}(1-\alpha)^n \quad (5)$$

In non-isothermal TGA experiments, the heating rate varies linearly with time (Mishra and Bhaskar, 2014):

$$\frac{dT}{dt} = \beta \quad (6)$$

where β is the heating rate (K min^{-1}). The conversion rate can be expressed as:

$$\frac{d\alpha}{dT} = \frac{d\alpha}{dt} \times \frac{1}{\beta} \quad (7)$$

Substituting equation (5) into (7) produces:

$$\frac{d\alpha}{dT} = \frac{A}{\beta} exp^{\left(-\frac{E}{RT}\right)} f(\alpha) \quad (8)$$

Integration of equation (8) from initial conditions yields (Vyazovkin *et al.,* 2011):

$$\int_0^\alpha \frac{d\alpha}{f(\alpha)} = g(\alpha) = \frac{A}{\beta} \int_{T_0}^{T} exp^{\left(-\frac{E}{RT}\right)}\ dT \quad (9)$$

where g(α) is the integral conversion function and T_0 is the initial temperature.

Kinetic Methods

Kissinger-Akahira-Sunose (KAS) Method

The KAS method (Kissinger, 1957; Akahira and Sunose, 1971), derived from equation (9), is expressed as:

$$ln\left(\frac{\beta}{T^2}\right) = ln\left(\frac{AE}{Rg(\alpha)}\right) - \frac{E}{RT} \quad (10)$$

A plot of $\ln(\beta/T^2)$ versus $1/T$ at different heating rates yields a straight line, with the slope equal to $-E/R$, enabling activation energy determination (Safana *et al.,* 2019).

Flynn-Wall-Ozawa (FWO) Method

The FWO method (Flynn and Wall, 1966; Ozawa, 1965) provides an alternative isoconversional approach:

$$ln\,\beta = ln(\frac{AE}{Rg(\alpha)}) - 5.331 - 1.052\ \frac{E}{RT} \qquad (11)$$

Plotting ln(β) against 1/T at various heating rates allows calculation of the apparent activation energy from the slope (−1.052E/R) at constant α values (Safana *et al.*, 2019; Mishra and Bhaskar, 2014).

Coats-Redfern (CR) Method

The CR method (Coats and Redfern, 1964) represents a comprehensive integral kinetic approach for describing mass loss mechanisms. Assuming 2RT/E → 0, equation (9) can be rearranged as:

$$ln(\frac{g(\alpha)}{T^2}) = ln(\frac{AR}{\beta E}) - \frac{E}{RT} \qquad (12)$$

A plot of ln[g(α)/T²] versus 1/T produces a straight line with slope −E/R and intercept yielding the pre-exponential factor A (Kuen-Song *et al.*, 1999). The appropriate kinetic mechanism is selected based on the highest coefficient of determination (R^2) (White *et al.*, 2011).

Kinetic Mechanisms

The theoretical expressions for g(α) the integral conversion function is derived by integrating the rate equation over the reaction coordinate α. Each model encodes a distinct physical assumption about how the solid-phase reaction proceeds. Two principal families of models are employed in biomass pyrolysis analysis: (i) Reaction Order Models, which assume homogeneous chemical kinetics governing the decomposition rate, and (ii) Diffusion Models, which assume that mass transfer through a growing product (char/ash) layer is the rate-controlling step. The Coats-Redfern (CR) method evaluates each g(α) function against experimental TGA data, and the model exhibiting the highest coefficient of determination (R^2) is selected as the dominant mechanism (Coats and Redfern, 1964). Tables 1and 2 presented the explanation of the two kinetic mechanisms that is the reaction order (Table 1) and diffusion models (Table 2).

Table 1. Kinetic Mechanism Models: g(α) Functions and Reaction Mechanism Classifications for Biomass Pyrolysis (Reaction Order Models) (White *et al.*, 2011; Vyazovkin *et al.*, 2011)

Code	Model Name	g(α) Expression	Mechanism Type	Physical Interpretation
F1	First-Order	$g(\alpha) = -\ln(1-\alpha)$	Reaction Order	Random nucleation and subsequent growth. Decomposition rate proportional to remaining unreacted fraction. Typical of cellulose-dominated biomass; chain-scission follows first-order decay.
F2	Second-Order	$g(\alpha) = (1-\alpha)^{-1} - 1$	Reaction Order	Two-body collision mechanism. Rate depends on the square of the unreacted fraction. Favored in lignin-rich biomass (e.g., PKS) due to complex cross-linked polymer networks requiring bimolecular interactions.
F3	Third-Order	$g(\alpha) = [(1-\alpha)^{-2} - 1]/2$	Reaction Order	Higher-order multi-body reaction. Produces the highest activation

Code	Model Name	g(α) Expression	Mechanism Type	Physical Interpretation
				energies among order models but typically exhibits lower R^2 fits for biomass pyrolysis, indicating less statistical suitability.

Table 2. Kinetic Mechanism Models: g(α) Functions and Reaction Mechanism Classifications for Biomass Pyrolysis (Diffusion Models) (White *et al.,* 2011; Vyazovkin *et al.,* 2011)

Code	Model Name	g(α) Expression	Mechanism Type	Physical Interpretation
D1	One-Way Transport	$g(\alpha) = \alpha^2$	Diffusion	Parabolic diffusion law. Rate-limiting step is one-dimensional diffusion through a flat product layer. Applicable to early-stage char formation where geometry is approximately planar.
D2	Two-Way Transport	$g(\alpha) = [(1-\alpha)\ln(1-\alpha)] + \alpha$	Diffusion	Valensi equation for two-dimensional (cylindrical) diffusion. Accounts for diffusion through a product layer surrounding a cylindrical particle; relevant to fibrous biomass structures such as EFB.
D3	Jander Equation (3D)	$g(\alpha) = [1 - (1-\alpha)^{\wedge}⅓]^2$	Diffusion	Three-dimensional diffusion through a spherical product shell (Jander equation). Exhibits the lowest activation energies (32.57–37.47 $kJmol^{-1}$) among all models, indicating significance in char combustion and the rate-limiting role of volatile diffusion through a growing ash/char barrier layer.
D4	Ginstling–Brounshtein	$g(\alpha) = 1 - (2\alpha/3) - (1-\alpha)^{\wedge}⅔$	Diffusion	Modified 3D diffusion model accounting for geometric contraction of the reactive interface during product layer growth. Provides high R^2 values at advanced conversion stages, reflecting its relevance in late-stage thermal decomposition of all three biomass types.

Experimental Procedure

Thermogravimetric analysis was conducted on three oil palm biomass samples: empty fruit bunch (EFB), mesocarp fiber (MF), and palm kernel shell (PKS). These residues are major by-products of the palm oil milling process and are generated in large quantities (Abdullah and Sulaiman, 2013; Sulaiman *et al.,* 2011). The samples were subjected to non-isothermal pyrolysis under inert atmosphere (N_2 at 80 ml min^{-1}) at multiple heating rates (5, 10, and 20 °C min^{-1}), consistent with the approach employed by Safana *et al.* (2019) for EFB and PKS. Average sample masses of 10.33 mg (EFB), 10.35 mg (MF), and 10.29 mg (PKS) were heated over the temperature range 30–850 °C. The kinetic parameters were calculated using the KAS, FWO, and CR methods at various conversion factors ranging from 0.1 to 0.7. The selection of the

best-fit mechanism was based on the highest regression coefficient (R^2) values (Vyazovkin *et al.*, 2011).

Results and Discussion

Thermogravimetric Analysis

The TGA and DTG profiles obtained for EFB, MF, and PKS at heating rates of 5, 10, and 20 °C min^{-1} under nitrogen atmosphere are presented in Figures 1 and 2, respectively. Average sample masses of 10.33 mg (EFB), 10.35 mg (MF), and 10.29 mg (PKS) were heated over the temperature range 30–850 °C. Analysis of the curves revealed three distinct decomposition zones for all three samples, irrespective of heating rate, corresponding to the onset and termination points of the DTG peaks, each indicative of the thermal breakdown of organic matter and volatiles (Luangkiattikhun *et al.*, 2008).

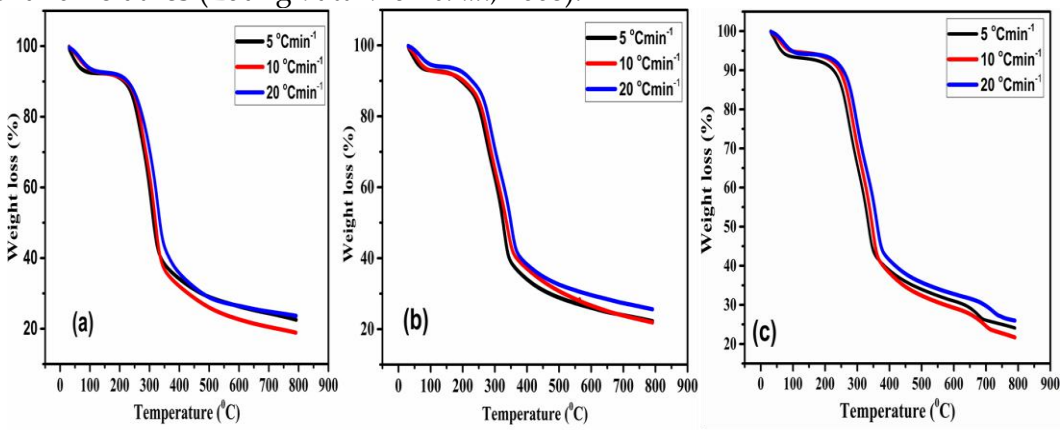

Figure 1. TGA profiles for oil palm biomass under N_2 (80 ml min^{-1}) at heating rates of 5, 10, and 20 °C min^{-1}: (a) EFB (10.33 mg), (b) MF (10.35 mg), and (c) PKS (10.29 mg).

Zone 1: Dehydration (30–250 °C): The first zone, spanning 30 to 250 °C, was characterized by moisture evaporation and dehydration for all three biomass samples across all heating rates. The mass loss in this zone was relatively minor and attributed primarily to the release of physically adsorbed and chemically bound water (Yang *et al.*, 2004).

Zone 2: Active Pyrolysis (200–360 °C): The second zone, occurring between 200 and 360 °C, represented the primary active pyrolysis stage in which the maximum weight loss was recorded for all samples due to oxidation and removal of volatile matter (Table 3). EFB exhibited the highest weight loss in this zone, attributable to its high volatile content (Safana *et al.*, 2019). DTG curves for PKS and MF displayed separate peaks for hemicellulose at approximately 300 °C and cellulose above 300 °C (Sulaiman and Abdullah, 2011), consistent with the literature on oil palm biomass. Specifically, the maximum degradation rate of cellulose was observed between 300 and 360 °C, while hemicellulose degraded between 270 and 300 °C across all three palm oil waste materials. Lignin degradation was observed up to 650 °C, with PKS demonstrating the greatest thermal resistance due to its high lignin content (Luangkiattikhun *et al.*, 2008).

Zone 3: Passive Pyrolysis / Char Combustion (340–800 °C): The third zone, from 340 to 800 °C, corresponded to char oxidation and the removal of residual volatiles. The temperature intervals and weight losses recorded for each zone at all three heating rates are summarized in Table 3. The total weight loss between 100 and 450 °C was 78.60%, 75.71%, and 98.50% for

EFB, MF, and PKS, respectively, reflecting the differences in the biochemical composition and volatile content of each biomass.

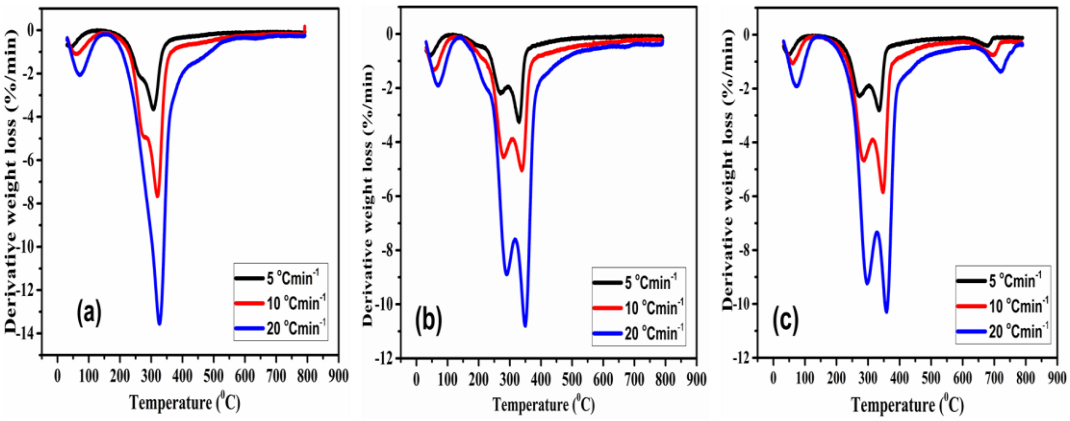

Figure 2. DTG profiles for oil palm biomass at heating rates of 5, 10, and 20 °C min^{-1}: (a) EFB, (b) MF, and (c) PKS.

Table 3. Temperature Intervals and Weight Loss for the Second and Third Decomposition Zones at Different Heating Rates

Sample	Heating Rate (°C min^{-1})	Second Zone Temperature (°C)	Third Zone Temperature (°C)	Weight Loss 2nd Zone (wt%)	Weight Loss 3rd Zone (wt%)
EFB	5	200–340	340–800	51.29	16.95
	10	200–340	340–800	52.35	19.47
	20	250–360	360–800	45.52	17.26
MF	5	220–340	340–800	46.21	18.90
	10	220–360	360–800	47.53	18.90
	20	250–360	360–800	43.20	18.24
PKS	5	220–340	340–800	43.04	22.90
	10	220–360	360–800	49.29	21.16
	20	250–360	360–800	40.21	23.82

Note: Weight losses are expressed as wt% of the initial sample mass.
Second zone = active pyrolysis; Third zone = passive pyrolysis/char combustion.

The peak temperatures recorded in the second (active pyrolysis) zone and the burnout temperatures for all samples at each heating rate are presented in Table 4. The highest peak temperature of 358 °C was recorded at 20 °C min^{-1} from PKS, reflecting its lignin-rich composition and greater thermal stability. EFB displayed the highest burnout temperature of 680 °C at 20 °C min^{-1}, followed by PKS at 650 °C and MF at 620 °C, suggesting that EFB requires the most energy for complete decomposition, consistent with the high activation energies subsequently determined by the isoconversional methods. A clear and consistent trend was observed across all three samples: as the heating rate increased from 5 to 20 °C min^{-1}, both the peak and burnout temperatures shifted to higher values. This thermal lag effect is a well-documented phenomenon in non-isothermal TGA studies arising from the kinetic delay between heat supply and sample response, and is in agreement with previously reported findings (Safana *et al.*, 2019; Luangkiattikhun *et al.*, 2008).

Table 4. Peak and Burnout Temperatures of EFB, MF, and PKS at Different Heating Rates

Sample	Heating Rate (°C min⁻¹)	Peak Temperature – Second Zone (°C)	Burnout Temperature (°C)
EFB	5	308	550
	10	320	600
	20	328	680
MF	5	330	530
	10	338	580
	20	349	620
PKS	5	336	550
	10	346	580
	20	358	650

Note: Peak temperature refers to the temperature of maximum mass loss rate (DTG peak) in the second (active pyrolysis) zone. Burnout temperature denotes the temperature at which decomposition is essentially complete.

Activation Energy Analysis by Model-Free Methods

The kinetic parameters derived from the KAS and FWO model-free methods are presented in Table 5. Both methods exhibited excellent agreement in activation energy values, validating the reliability of the isoconversional approach (Vyazovkin *et al.*, 2011; Mishra and Bhaskar, 2014). The linear regression plots of 1/T versus $\ln(\beta/T^2)$ for KAS and $\ln(\beta)$ for FWO at different conversion factors demonstrated strong correlations, with R^2 values predominantly exceeding 0.96, consistent with the findings of Safana *et al.* (2019) for EFB and PKS.

Table 5. Activation Energy (E) and Pre-Exponential Factors (A) Determined by KAS and FWO Methods

Sample	Conversion (a)	E_{KAS} (kJmol^{-1})	R^2	A (min^{-1})	E_{FWO} (kJmol^{-1})	R^2	A (min^{-1})
EFB	0.1	167.19	0.9642	4.82×10^{15}	167.28	0.9675	5.08×10^{15}
	0.2	184.07	0.9849	8.14×10^{16}	183.65	0.9862	7.66×10^{16}
	0.3	187.95	0.9995	7.62×10^{16}	187.62	0.9996	7.32×10^{16}
	0.4	196.30	0.9927	2.16×10^{17}	195.77	0.9933	2.00×10^{17}
	0.5	194.36	0.9973	8.45×10^{16}	194.11	0.9976	8.28×10^{16}
	0.6	203.02	0.9999	2.92×10^{17}	202.53	0.9999	2.73×10^{17}
	0.7	**213.38**	0.9939	3.21×10^{17}	**212.88**	0.9944	3.02×10^{17}
MF	0.1	136.13	0.9968	4.49×10^{12}	150.43	0.9862	1.30×10^{14}
	0.2	183.50	0.9947	7.76×10^{16}	183.11	0.9952	7.35×10^{16}

	0.3	208.48	0.9982	6.80×10^{18}	207.13	0.9983	5.34×10^{18}
	0.4	**210.78**	0.9978	3.16×10^{18}	**209.63**	0.9958	2.59×10^{18}
	0.5	209.88	0.9919	9.01×10^{17}	209.04	0.9926	7.89×10^{17}
	0.6	187.16	0.9381	4.70×10^{15}	187.63	0.9439	5.36×10^{15}
	0.7	198.02	0.8186	1.07×10^{16}	167.63	0.8475	1.86×10^{13}
PKS	0.1	103.15	0.9716	9.65×10^{8}	132.66	0.9957	8.96×10^{11}
	0.2	138.50	0.9857	1.70×10^{12}	140.46	0.9874	2.86×10^{12}
	0.3	155.18	0.9907	3.39×10^{13}	156.60	0.9917	4.88×10^{13}
	0.4	156.03	0.9720	1.73×10^{13}	157.71	0.9750	2.63×10^{13}
	0.5	169.69	0.9954	1.41×10^{14}	170.99	0.9959	1.92×10^{14}
	0.6	170.98	0.9983	1.06×10^{14}	172.44	0.9985	1.50×10^{14}
	0.7	**193.35**	0.9666	8.02×10^{14}	**196.43**	0.9699	1.02×10^{15}

Note: $\mathbf{E_{KAS}}$ **(kJmol^{-1})** *and* $\mathbf{E_{FWO}}$**(kJmol^{-1})** *values determined at constant conversion factors (α) from linear regression of isoconversional plots. R^2 values indicate the quality of the linear fit.*

The maximum activation energies for EFB (213.38 kJmol^{-1} by KAS, 212.88 kJmol^{-1} by FWO) occurred at a conversion factor of 0.7, indicating substantial energy requirements for the final stages of pyrolysis. Similarly, PKS exhibited maximum activation energies of 193.35 kJmol^{-1} (KAS) and 196.43 kJmol^{-1} (FWO) at $\alpha = 0.7$, which closely mirrors the values reported by Safana *et al.* (2019) for palm shell, confirming reproducibility. In contrast, MF demonstrated peak activation energies of 210.78 kJmol^{-1} (KAS) and 209.63 kJmol^{-1} (FWO) at an earlier conversion stage ($\alpha = 0.4$), suggesting different decomposition characteristics consistent with the earlier DTG peak temperature shift observed for MF.

A consistent trend observed across all samples was the progressive increase in activation energy with increasing conversion factor, reflecting the sequential decomposition of hemicellulose (220–315 °C), cellulose (315–400 °C), and the thermally recalcitrant lignin (160–900 °C) (Yang *et al.,* 2004; Cai *et al.,* 2013). This pattern aligns with the three decomposition zones identified in the TGA/DTG analysis (Section 3.1). PKS consistently exhibited the lowest activation energies, positioning it as the most favorable feedstock for pyrolysis, in agreement with Safana *et al.* (2019). The pre-exponential factors (A) ranged from 10^8 to 10^{18} min^{-1} and exhibited the kinetic compensation effect (Vyazovkin *et al.,* 2011), with higher A values corresponding to higher E values.

Coats-Redfern Method Analysis

The apparent activation energies and kinetic mechanisms determined by the Coats-Redfern method (Coats and Redfern, 1964) at 20 °C min^{-1} are presented in Table 6. This heating rate provided the best-fit mechanisms based on R^2 values, in agreement with Chen *et al.* (2014), who noted the significant influence of heating rate on kinetic parameter estimation.

Table 6. Apparent Activation Energies and Pre-Exponential Factors by Coats-Redfern Method (20 °C min^{-1})

Sample	Mechanism	E ($kJmol^{-1}$)	R^2	A (min^{-1})
EFB	F1	45.97	**0.9917**	3.92×10^{1}
	F2	65.27	0.9783	4.47×10^{3}
	F3	88.51	0.9614	1.17×10^{6}
	D1	71.50	0.9933	3.70×10^{3}
	D2	80.18	0.9950	1.54×10^{4}
	D3	35.50	0.9935	1.83
	D4	83.62	0.9952	7.83×10^{3}
MF	F1	41.13	**0.9964**	1.17×10^{1}
	F2	56.50	0.9915	5.47×10^{2}
	F3	74.71	0.9792	4.61×10^{4}
	D1	67.15	0.9879	1.27×10^{3}
	D2	74.43	0.9927	3.81×10^{3}
	D3	32.57	0.9902	8.58×10^{-1}
	D4	77.25	0.9941	1.69×10^{3}
PKS	F1	44.84	0.9925	2.21×10^{1}
	F2	57.61	**0.9958**	5.26×10^{2}
	F3	72.35	0.9922	1.90×10^{4}
	D1	77.83	0.9831	9.54×10^{3}
	D2	84.32	0.9876	2.31×10^{4}
	D3	37.47	0.9840	2.26
	D4	86.76	0.9891	9.26×10^{3}

Note: Highlighted cells (shaded blue) indicate the dominant kinetic mechanism for each biomass sample as determined by the highest R^2 value.

Reaction Order Models

Within the reaction order models, F3 consistently yielded the highest activation energies (88.51, 74.71, and 72.35 $kJmol^{-1}$ for EFB, MF, and PKS respectively), but mechanism selection is based on R^2 rather than activation energy magnitude (White *et al.,* 2011). Based on R^2 values, F1 emerged as the dominant model for EFB (R^2 = 0.9917) and MF (R^2 = 0.9964), while F2 provided the best fit for PKS (R^2 = 0.9958). This correlates directly with the biochemical composition, EFB and MF have higher cellulose content, leading to first-order chain-scission kinetics (Cai *et al.,* 2013), while PKS's higher lignin content, as evidenced by its high burnout temperature in the TGA analysis, necessitates second-order bimolecular decomposition pathways (Safana *et al.,* 2019; Luangkiattikhun *et al.,* 2008). The lower activation energies from the CR method compared to KAS/FWO reflect the CR method's focus on the primary decomposition zone (Zone 2), whereas isoconversional methods integrate the full conversion range (Vyazovkin *et al.,* 2011).

Diffusion Models

Analysis of diffusion models revealed a systematic increase in activation energies from D1 to D4, with the notable exception of D3. For EFB: 71.50 (D1) to 83.62 kJmol^{-1} (D4), with D3 at only 35.50 kJmol^{-1}. For MF: 67.15 to 77.25 kJmol^{-1}, with D3 at 32.57 kJmol^{-1}. For PKS: 77.83 to 86.76 kJmol^{-1}, with D3 at 37.47 kJmol^{-1}. The substantially lower activation energy of the D3 Jander model across all samples is consistent with the passive pyrolysis zone (Zone 3) observed in the TGA profiles, where three-dimensional diffusion through a growing char/ash shell becomes the rate-controlling step (Islam *et al.,* 2016; White *et al.,* 2011). The D4 Ginstling-Brounshtein model also showed consistently high R^2 values, reflecting its relevance in the advanced stages of thermal decomposition (Vyazovkin *et al.,* 2011).

CONCLUSION

This comprehensive kinetic study of oil palm biomass pyrolysis has successfully characterized the thermal decomposition behavior of EFB, MF, and PKS through TGA/DTG analysis and multiple kinetic methods, extending the foundational work of Safana *et al.* (2019) by incorporating MF and applying the Coats-Redfern model-fitting approach. TGA and DTG analysis identified three distinct decomposition zones, dehydration (30–250 °C), active pyrolysis (200–360 °C), and passive pyrolysis/char combustion (340–800 °C), for all three biomass types. The highest weight loss in the active zone was recorded for EFB due to its elevated volatile content. PKS demonstrated the highest peak temperature (358 °C at 20 °C min^{-1}) and high thermal resistance in the char zone, consistent with its elevated lignin content. Burnout temperatures increased with heating rate for all samples, with EFB recording the highest burnout temperature of 680 °C.

The model-free methods (KAS and FWO) revealed maximum activation energies of 213.38 kJmol^{-1} (EFB), 210.78 kJmol^{-1} (MF), and 193.35 kJmol^{-1} (PKS), with excellent agreement between both methods validating the reliability of isoconversional analysis. PKS demonstrated the most favorable thermal characteristics with the lowest activation energies, positioning it as the optimal feedstock for efficient thermochemical conversion. The Coats-Redfern analysis identified first-order kinetics as the dominant mechanism for EFB and MF (higher cellulose content) and second-order kinetics for PKS (lignin-rich composition). Among diffusion models, D3 exhibited the lowest activation energies (32.57–37.47 kJmol^{-1}), confirming its significance in char combustion.

REFERENCES

Abdullah, N., & Sulaiman, F. (2013). The oil palm wastes in Malaysia. In M. D. Matovic (Ed.), *Biomass now – Sustainable growth and use* (pp. 75–93). IntechOpen.

Akahira, T., & Sunose, T. (1971). Method of determining activation deterioration constant of electrical insulating materials. *Research Report, Chiba Institute of Technology (Science and Technology), 16*, 22–31.

Bridgwater, A. V. (2012). Review of fast pyrolysis of biomass and product upgrading. *Biomass and Bioenergy, 38*, 68–94. https://doi.org/10.1016/j.biombioe.2011.01.048

Cai, J., Wu, W., Liu, R., & Huber, G. W. (2013). A distributed activation energy model for the pyrolysis of lignocellulosic biomass. *Green Chemistry, 15*(5), 1331–1340. https://doi.org/10.1039/c3gc36958g

Chen, D., Zhou, J., & Zhang, Q. (2014). Effects of heating rate on slow pyrolysis behavior, kinetic parameters and products properties of moso bamboo. *Bioresource Technology, 169*, 313–319. https://doi.org/10.1016/j.biortech.2014.07.009

Coats, A. W., & Redfern, J. P. (1964). Kinetic parameters from thermogravimetric data. *Nature, 201*, 68–69. https://doi.org/10.1038/201068a0

Damartzis, T., & Zabaniotou, A. (2011). Thermochemical conversion of biomass to second generation biofuels through integrated process design—A review. *Renewable and Sustainable Energy Reviews, 15*(1), 366–378. https://doi.org/10.1016/j.rser.2010.08.003

Di Blasi, C. (2008). Modeling chemical and physical processes of wood and biomass pyrolysis. *Progress in Energy and Combustion Science, 34*(1), 47–90. https://doi.org/10.1016/j.pecs.2006.12.001

Flynn, J. H., & Wall, L. A. (1966). A quick, direct method for the determination of activation energy from thermogravimetric data. *Journal of Polymer Science Part B: Polymer Letters, 4*(5), 323–328. https://doi.org/10.1002/pol.1966.110040504

Islam, M. A., Asif, M., & Hameed, B. H. (2015). Pyrolysis kinetics of raw and hydrothermally carbonized Karanj (Pongamia pinnata) fruit hulls via thermogravimetric analysis. *Bioresource Technology, 179*, 227–233. https://doi.org/10.1016/j.biortech.2014.12.038

Islam, M. A., Asif, M., & Hameed, B. H. (2016). A thermogravimetric analysis of the combustion kinetics of karanja (Pongamia pinnata) fruit hulls char. *Bioresource Technology, 200*, 335–341. https://doi.org/10.1016/j.biortech.2015.10.047

Kissinger, H. E. (1957). Reaction kinetics in differential thermal analysis. *Analytical Chemistry, 29*(11), 1702–1706. https://doi.org/10.1021/ac60131a045

Kuen-Song, L., Wang, H. P., Liu, S.-H., Chang, N.-B., Huang, Y.-J., & Wang, H.-C. (1999). Pyrolysis kinetics of refuse-derived fuel. *Fuel Processing Technology, 60*, 103–110. https://doi.org/10.1016/S0378-3820(99)00021-1

Kumar, A., Wang, L., Dzenis, Y. A., Jones, D. D., & Hanna, M. A. (2008). Thermogravimetric characterization of corn stover as gasification and pyrolysis feedstock. *Biomass and Bioenergy, 32*(5), 460–467. https://doi.org/10.1016/j.biombioe.2007.11.004

Li, Y., Xing, X., Xu, B., Xing, Y., Zhang, X., Yang, J., & Xing, J. (2017). Effect of the particle size on co-combustion of municipal solid waste and biomass briquette under N_2/O_2 and CO_2/O_2 atmospheres. *Energy & Fuels, 31*(1), 932–940. https://doi.org/10.1021/acs.energyfuels.6b02574

Luangkiattikhun, P., Tangsathitkulchai, C., & Tangsathitkulchai, M. (2008). Non-isothermal thermogravimetric analysis of oil-palm solid wastes. *Bioresource Technology, 99*(5), 986–997. https://doi.org/10.1016/j.biortech.2007.03.001

Mishra, G., & Bhaskar, T. (2014). Non isothermal model free kinetics for pyrolysis of rice straw. *Bioresource Technology, 169*, 614–621. https://doi.org/10.1016/j.biortech.2014.07.045

Nussbaumer, T. (2003). Combustion and co-combustion of biomass: Fundamentals, technologies, and primary measures for emission reduction. *Energy & Fuels, 17*, 1510–1521. https://doi.org/10.1021/ef030031q

Ozawa, T. (1965). A new method of analyzing thermogravimetric data. *Bulletin of the Chemical Society of Japan, 38*(11), 1881–1886. https://doi.org/10.1246/bcsj.38.1881

Safana, A. A., Abdullah, N., & Sulaiman, F. (2019). A study of pyrolysis kinetics of palm shell and empty fruit bunches via thermogravimetric analysis (TGA). *Academia Journal of Scientific Research, 7*(2), 155–162. https://doi.org/10.15413/ajsr.2018.0163

Saidur, R., Abdelaziz, E. A., Demirbas, A., Hossain, M. S., & Mekhilef, S. (2011). A review on biomass as a fuel for boilers. *Renewable and Sustainable Energy Reviews, 15*(5), 2262–2289. https://doi.org/10.1016/j.rser.2011.02.015

Slopiecka, K., Bartocci, P., & Fantozzi, F. (2011). Thermogravimetric analysis and kinetic study of poplar wood. In *Proceedings of the Third International Conference on Applied Energy* (pp. 1687–1698). Applied Energy.

Sulaiman, F., & Abdullah, N. (2011). Optimum conditions for maximising pyrolysis liquids of oil palm empty fruit bunches. *Energy, 36*(5), 2352–2359. https://doi.org/10.1016/j.energy.2010.12.067

Sulaiman, F., Abdullah, N., Gerhauser, H., and Shariff, A. (2011). An outlook of Malaysian energy, oil palm industry and its utilization of wastes as useful resources. Biomass and Bioenergy, 35(9): 3775–3786.

Vyazovkin, S., Burnham, A. K., Criado, J. M., Pérez-Maqueda, L. A., Popescu, C., & Sbirrazzuoli, N. (2011). ICTAC Kinetics Committee recommendations for performing kinetic computations on thermal analysis data. *Thermochimica Acta, 520*(1–2), 1–19. https://doi.org/10.1016/j.tca.2011.03.034

White, J. E., Catallo, W. J., & Legendre, B. L. (2011). Biomass pyrolysis kinetics: A comparative critical review with relevant agricultural residue case studies. *Journal of Analytical and Applied Pyrolysis, 91*(1), 1–33. https://doi.org/10.1016/j.jaap.2011.01.004

Yang, Y. B., Sharifi, V. N., & Swithenbank, J. (2004). Effect of air flow rate and fuel moisture on the burning behaviours of biomass and simulated municipal solid wastes in packed beds. *Fuel, 83*(11–12), 1553–1562. https://doi.org/10.1016/j.fuel.2004.01.016